

This discussion paper is/has been under review for the journal *Atmospheric Chemistry and Physics (ACP)*. Please refer to the corresponding final paper in *ACP* if available.

**Multi-phase MBL
chemistry**

D. Lowe et al.

Modelling multi-phase halogen chemistry in the remote marine boundary layer: investigation of the influence of aerosol size resolution on predicted gas- and condensed-phase chemistry

D. Lowe, D. Topping, and G. McFiggans

School of Earth, Atmospheric and Environmental Science, University of Manchester, Manchester, UK

Received: 4 February 2009 – Accepted: 5 February 2009 – Published: 2 March 2009

Correspondence to: D. Lowe (douglas.lowe@manchester.ac.uk)

Published by Copernicus Publications on behalf of the European Geosciences Union.

Title Page

Abstract

Introduction

Conclusions

References

Tables

Figures

⏪

⏩

◀

▶

Back

Close

Full Screen / Esc

Printer-friendly Version

Interactive Discussion



Abstract

A coupled box model of photochemistry and aerosol microphysics which explicitly accounts for size-dependent chemical properties of the condensed-phase has been developed to simulate the multi-phase chemistry of chlorine, bromine and iodine in the marine boundary layer (MBL). The model contains separate seasalt and non-seasalt modes, each of which may be composed of 1–16 size-sections. By comparison of gaseous and aerosol compositions predicted using different size-resolutions with both fixed and size-dependent aerosol turnover rates, it was found that, for halogen-activation processes, the physical property initialisation of the aerosol-mode has a significant influence on gas-phase chemistry. Failure to adequately represent the appropriate physical properties can lead to substantial errors in gas-phase chemistry. The size-resolution of condensed-phase composition has a less significant influence on gas-phase chemistry.

1 Introduction

Recent measurements have shown that halogens can play a major role in the destruction of tropospheric ozone – causing up to 50% of the ozone loss in the remote marine boundary layer (MBL) (Read et al., 2008). It has been shown that seasalt particles generated from the sea surface via wind shear are the major source of inorganic halogen species in the MBL (cf. Keene et al., 1999; Sander et al., 2003) and size-segregated measurements of aerosols in the MBL have shown that most seasalt aerosol particles have a pH of 3.5–4.5, varying across the particle size-range (Keene et al., 2002, 2004). It may be expected then, that to investigate the causes and impacts of such variations in composition, a size-resolved aerosol model must be used.

Detailed MBL mixed-phase chemistry has historically been studied using photochemical box models which treat the condensed-phase as a simple reactive volume, using representative aerosol microphysical properties to determine gas-aerosol ex-

Multi-phase MBL chemistry

D. Lowe et al.

Title Page

Abstract

Introduction

Conclusions

References

Tables

Figures

◀

▶

◀

▶

Back

Close

Full Screen / Esc

Printer-friendly Version

Interactive Discussion



change rates but not allowing them to evolve through time (e.g. Model Of Chemistry Considering Aerosols, MOCCA, Sander and Crutzen, 1996). Recent work to improve the treatment of the condensed-phase have focussed on one of two aspects: either size-resolved chemistry or size-resolved aerosol microphysics.

5 The first approach simply consists of increasing the number of condensed-phases, giving each separate microphysical properties which relate to a size-resolved aerosol distribution, but still without considering how these properties change with time (although replenishment of condensed-phase chemical constituents by aerosol turn-over is generally incorporated). This method has been used in the study of Pszenny et al.
10 (2004), who adapted MOCCA to use 14 separate condensed-phases, 7 seasalt and 7 non-seasalt; and that of Toyota et al. (2001) using SEAMAC (size-SEgregated Aerosol model for Marine Air Chemistry), which consists of 8 separate condensed-phases, all seasalt, and uses the ASAD chemical solver (Carver et al., 1997).

The second approach involves overlaying the mixed-phase chemistry scheme onto
15 a full aerosol microphysical scheme, which is used to determine the aerosol properties needed by the chemistry scheme. This approach has been followed by von Glasow et al. (2002), who created their 1-D column model MISTRA-MPIC (Micro-physical STRAtus model – Max-Planck-Institut für Chemie version) by combining a detailed chemistry scheme with the aerosol microphysical model of (Bott et al., 1996).
20 Condensed-phase chemistry is calculated using two sections, one seasalt and one “sulphate”; the microphysical properties of each being determined by combining the properties of all aerosol sections larger than $0.5\ \mu\text{m}$ for the seasalt mode, and all sections smaller than $0.5\ \mu\text{m}$ for the “sulphate” mode.

25 The aim of this paper is to investigate the relative importance of size-resolution of both condensed-phase chemistry and aerosol microphysics to the chemistry in the remote MBL. A previous modelling study (Toyota et al., 2001) has shown that gas-phase chemistry is dependent on the size-resolution of the aerosol mode but it is unclear from that work if the dependence is due to microphysical or chemical influences. An intention of the current work is to clarify the causes of this dependence.

**Multi-phase MBL
chemistry**

D. Lowe et al.

Title Page

Abstract

Introduction

Conclusions

References

Tables

Figures

◀

▶

◀

▶

Back

Close

Full Screen / Esc

Printer-friendly Version

Interactive Discussion



2 Methods

In order to address these questions a highly detailed aerosol model (MANIC: Microphysical Aerosol Numerical model Incorporating Chemistry) has been developed, which can treat both condensed-phase chemistry and aerosol microphysics at a high-resolution. MANIC is a zero-dimensional aerosol model designed for studying multi-phase chemistry. The Kinetic PreProcessor (KPP) program (Damian et al., 2002) is used to construct a system of ODEs representing the chemical continuity equations which are solved using the 3rd order Rosenbrock solver packaged with KPP. All gas and condensed-phase chemical reactions are solved in the same time-step; avoiding any errors associated with operator-splitting (cf. Sportisse, 2000). For this same reason the physical processes affecting the condensed-phase are solved within the same time-step as the chemistry. The microphysical properties of the condensed-phase are re-calculated for every internal time-step taken by the Rosenbrock solver; physical properties of the particles, such as mass and density, are calculated directly from the condensed chemical species. Aerosol particles are moved between size-sections using the Moving Centre method (Jacobson, 1997); the size-distributions being recalculated every 5 min of model time (the internal time-steps of the Rosenbrock solver are allowed to grow up to this limit).

The multi-phase chemistry scheme is based on that of Pechtl et al. (2006), with several updates (see supplementary material: <http://www.atmos-chem-phys-discuss.net/9/5289/2009/acpd-9-5289-2009-supplement.pdf>). The kinetics of gaseous halogen reactions are the subject of substantial ongoing research, but any changes to the scheme used here will not substantially change the conclusions of the current work. The condensed phase major ions (H^+ - Na^+ - NH_4^+ - HSO_4^- - SO_4^{2-} - NO_3^- - Cl^-) are treated in a non-ideal manner using PD-FiTE (Topping et al., 2009) to calculate the vapour pressures of HNO_3 , HCl and NH_3 as well as the activity coefficients for the dissociation of HSO_4^- and the aforementioned condensed-species. All other condensed-phase species are treated in an ideal manner (as is the above system for solutions with a pH greater

Title Page

Abstract

Introduction

Conclusions

References

Tables

Figures

◀

▶

◀

▶

Back

Close

Full Screen / Esc

Printer-friendly Version

Interactive Discussion



than 7). Midday photolysis rates are taken from Sander and Crutzen (1996), and adjusted for time of day using a simple scheme included with KPP. Mass transfer between the gas- and condensed-phases is controlled by the mass transfer rate k_t (Schwartz, 1986):

$$k_t = \left(\frac{r^2}{3D_g} + \frac{4r}{3\bar{v}\alpha} \right)^{-1}, \quad (1)$$

where r is the wet droplet radius, D_g is gas-phase diffusivity, \bar{v} is mean molecular speed, and α is accommodation coefficient. The mass transfer for each species is split into its constituent forward and backward reactions and solved in the same time-step as the chemistry (cf. Kerkweg et al., 2007).

Particle formation and coagulation are not treated in the current model. Particle turnover is simulated using a deposition rate, which can be size-dependent or not, matched exactly by an emission rate – so preserving aerosol number. The size-dependent turnover rate, $(\tau_s)^{-1}$, is estimated according to the dry and wet deposition processes:

$$(\tau_s)^{-1} = \left(\frac{Z_{\text{mbl}}}{v_d} \right)^{-1} + (\tau_{\text{wet}})^{-1}, \quad (2)$$

after Toyota et al. (2001). Z_{mbl} is the height of the MBL (=1000 m), and the size-dependent dry deposition velocity, v_d , is based on the model of Slinn and Slinn (1980) (assuming 9 m s^{-1} surface wind speed and neutral static stability). Wet deposition is assumed to give a particle lifetime, τ_{wet} , of 8 days. For this study we will represent the condensed-phase using two externally mixed aerosol modes, each of which could have a variety of different size resolutions: either 1, 2, 4, 8, or 16 sections.

The model is initialised with the gas-phase mixing ratios shown in Table 1; of these species only NH_3 is fixed. The gas-phase source terms (Table 2) represent two separate processes: emission of gas-phase species from the sea-surface; and the entrainment of air from the free troposphere into the MBL. The source terms for the iodine

[Title Page](#)[Abstract](#)[Introduction](#)[Conclusions](#)[References](#)[Tables](#)[Figures](#)[◀](#)[▶](#)[◀](#)[▶](#)[Back](#)[Close](#)[Full Screen / Esc](#)[Printer-friendly Version](#)[Interactive Discussion](#)

compounds represent the former process. Entrainment from the free troposphere is used for the NO and ozone source terms; a fixed ozone mixing ratio in the free troposphere of 52 nmol mol^{-1} is used, while all other gas-phase species are assumed to have the same mixing ratios as in the MBL. The gas-phase sink terms (Table 3) represent deposition at the sea-surface. Without a condensed-phase these initial and boundary conditions produce ozone night-time maxima, and day-time minima, of 34 and 32 nmol mol^{-1} , respectively (not shown).

The non-seasalt mode used in this study is a simple log-normal distribution, with parameters given in Table 4, and has a dry composition of 32% $(\text{NH}_4)_2\text{SO}_4$, 64% NH_4HSO_4 and 4% NH_4NO_3 . For the seasalt mode a pseudo-lognormal, bi-modal, distribution (Porter and Clarke, 1997) linearly scaled to yield $15 \mu\text{g m}^{-3}$ of particulate NaCl (after Toyota et al., 2001) is chosen. This represents a seasalt loading typical of higher wind-speed conditions close to the sea surface (cf. Graedel and Keene, 1995), chosen in order to exaggerate the magnitude of any size-resolution dependent effects which may occur. The dry composition of the seasalt mode is 99.4317% NaCl, 0.1491498% NaBr, $1.372178 \times 10^{-5}\%$ NaI, $4.812565 \times 10^{-5}\%$ NaIO_3 , and 0.4176193% NaHCO_3 . Organic aerosol constituents are not included in this study, but MANIC may be expanded to incorporate treatment of representative organic material on the availability of the extended PD-FiTE thermodynamic module (Topping et al., 2009). The condensed-phase chemistry scheme is simplified by lumping together all (unreactive) cations as Na^+ (von Glasow et al., 2002). Similarly the initial composition of the seasalt mode has been simplified by not including sulphate (which is assumed to be unreactive), although sulphate is still allowed to condense onto the this mode. These simplifications, however, will not affect the conclusions of this study.

To generate the various discrete aerosol distributions used from these continuous distributions the given number distributions are first discretised into 128 sections. The (dry) surface area and volume for each section are then determined and recombined to create the 1, 2, 4, 8, or 16 section distributions. Only two of the three moments (number, surface area, and mass) of the aerosol-distribution can be preserved when calcu-

[Title Page](#)[Abstract](#)[Introduction](#)[Conclusions](#)[References](#)[Tables](#)[Figures](#)[◀](#)[▶](#)[◀](#)[▶](#)[Back](#)[Close](#)[Full Screen / Esc](#)[Printer-friendly Version](#)[Interactive Discussion](#)

**Multi-phase MBL
chemistry**

D. Lowe et al.

Title Page

Abstract

Introduction

Conclusions

References

Tables

Figures

I◀

▶I

◀

▶

Back

Close

Full Screen / Esc

Printer-friendly Version

Interactive Discussion



lating these reduced resolution distributions. Thus there are three possible initialisation types: those preserving number and volume (N/V); number and surface area (N/S); and surface area and volume (S/V). The differences in the seasalt size-distribution for each of these initialisation types are shown in Fig. 1 and given in Table 5. The differences between initialisations for the 16-section distributions are of the order of a few percent, and so we shall treat these as an accurate reference representation of the continuous distribution. As the size-resolution of aerosol phase is reduced these discrete representations become less realistic. For the N/V initialisation, the seasalt dry surface area is too large and it is expected in model runs using this initialisation that chemical exchange between the gas- and condensed-phase would be too fast. For the N/S initialisation the seasalt dry volume is too low, reducing the total aerosol mass. It may be expected that this will reduce the halogen source from the condensed-phase. For the S/V initialisation the total particle number is too low; however this has no influence on the processes under investigation in the current work. It may therefore be expected that this will have no effect on the model runs.

All model runs are started with the initial conditions described above, and given 10 days spin-up time, which is the order of time scale required for all processes to stabilise to give a steady state diurnal profile. Whilst it is recognised that this is a somewhat unrealistic tropospheric residence time, it is required because all processes initiate a perturbation at time $t=0$, hence the model initialisations are far from steady-state. This is not the case in the real atmosphere, where a steady-state would be achieved in a much shorter time scale. The trends in all species are similar after, say, 3 or 4 days; but full stability in the results is exhibited after 10 days.

For all simulations described below a 1-section, S/V initialised, non-seasalt mode, with a size-independent turnover rate of 7 days⁻¹ is used. Model runs have been made to examine the influence of size-resolution in the non-seasalt model on the testcase results. For these clean marine conditions, however, the resolution dependence of this mode is minimal (not shown), and so for the discussion below focuses purely on the seasalt mode.

3 Results and discussion

3.1 Aerosol initialisation, size resolution and chemistry interactions

In Figures 2 and 3 the percentage ozone lost via autocatalytic halogen cycles, and gas-phase mixing ratios of key species are respectively shown for the fixed aerosol-turnover scenario showing a comparison of the three different initialisation techniques for the 1-section seasalt mode and the S/V initialised 16-section seasalt mode (all model runs are made with the same S/V initialised 1-section non-seasalt mode). The differences in gas-phase composition between the different initialisations methods for the 16-section seasalt mode are minor (<2%, not shown), supporting the assumption that using a 16-section resolution is a reasonable representation of the continuous distribution.

The differences in gas-phase chemistry between the S/V initialised 1-section and 16-section seasalt modes are generally minor (Fig. 3), with ozone levels within the 1-section model $\approx 0.05\%$ greater than those of the 16-section model. The observed changes in the gas-phase chemistry for the N/S initialised seasalt mode are, as may be expected from a lower seasalt mass loading: decreased gaseous mixing ratios of chlorine and bromine compounds (due to the lower mass of the seasalt source for these compounds) and increased levels of gaseous iodine compounds (due to the reduced size of the aerosol sink for iodine). These changes lead to a slight decrease in ozone destruction (ozone levels are $\approx 2\%$ higher). Likewise the changes in gas-phase chemistry for the N/V initialised seasalt mode are, as might be expected from increasing the surface-area across which the gas and condensed components interact: levels of gas-phase active chlorine and bromine compounds are higher – owing to increased rates of outgassing from the seasalt source term and also higher rates of heterogeneous processing. Active iodine compound levels are also slightly increased, again resulting from the increased processing rates. These changes lead to a marked increase in ozone destruction (ozone levels are $\approx 5\%$ lower).

The size-dependence of the major components of the seasalt mode is shown in Fig. 4. Of the 1-section seasalt representations it is evident that the S/V and N/V initial-

Title Page

Abstract

Introduction

Conclusions

References

Tables

Figures

◀

▶

◀

▶

Back

Close

Full Screen / Esc

Printer-friendly Version

Interactive Discussion



[Title Page](#)[Abstract](#)[Introduction](#)[Conclusions](#)[References](#)[Tables](#)[Figures](#)[◀](#)[▶](#)[◀](#)[▶](#)[Back](#)[Close](#)[Full Screen / Esc](#)[Printer-friendly Version](#)[Interactive Discussion](#)

isations best replicate the composition of the bulk mode of the higher resolution seasalt modes. As the size-resolution of the seasalt mode is increased the development of size-dependent structures in the seasalt composition become apparent. This is distinguishable in the 4-section model, but best resolved in the 8- and 16-section model runs. The developing features of the size-dependent composition are as expected; with the highest mixing ratios of those species which condense from the gas-phase (i.e. sulphuric and nitric acids, and iodine) in the smallest particles, while those species whose main source-term is the seasalt mode (i.e. chlorine) are most concentrated in the largest particles. In this context bromine is a special case – its main source term is the seasalt mode; but, once a steady state has been reached, the bromine content of the gas-phase is greater than that of the condensed-phase. These two bromine sources reinforce each other at the centre of the seasalt distribution, leading to a maximum in bromine mixing ratios during the day at these sizes of the distribution. This distribution pattern of bromine is only observed in the size-independent turnover scenario. When more realistic turnover rates are used these, as will be shown below, dominate the distribution of bromine across the particle size-range.

Gas-phase nitric acid mixing ratios are not so well captured using the 1-section seasalt modes, even when using the S/V initialisation (Fig. 3). However this discrepancy disappears when seasalt modes consisting of 2 or more sections are used (not shown). It is postulated that this difference occurs because the uptake of HNO_3 is strongly dependent on the acidity of the solution, and in the higher resolution seasalt modes is slowed by increasing acidity of the smallest seasalt particles (Fig. 4). In the 1-section model, however, the bulk of the seasalt mode absorbs the increase in acidity, so that the uptake of HNO_3 is not slowed.

3.2 Aerosol microphysics, size resolution and chemistry interactions

Model behaviour with more atmospherically realistic size-dependent turnover rates for the seasalt mode is now investigated. Figure 5 shows the gas-phase halogen compositions for the 1- to 16-section seasalt modes, where the seasalt turnover rates are calcu-

[Title Page](#)[Abstract](#)[Introduction](#)[Conclusions](#)[References](#)[Tables](#)[Figures](#)[◀](#)[▶](#)[◀](#)[▶](#)[Back](#)[Close](#)[Full Screen / Esc](#)[Printer-friendly Version](#)[Interactive Discussion](#)

lated on-line using Eq. (2). Ozone destruction is generally less for the lower resolution models – as are bromine and chlorine compound levels (while iodine compound levels are higher). This general trend can be attributed to the decrease in the bulk seasalt turnover rates with decreasing size-resolution (Table 6). This relationship breaks down for the 8- and 16-section models, but is consistent across the rest of the resolution range.

For this reason a fixed turnover lifetime of 0.57 days was used for the studies presented in Sect. 3.1 – based on the volumetrically averaged turnover rate of the 16-section model. Comparison of the 1-section seasalt model using this fixed turnover lifetime with the 16-section seasalt model using size-dependent turnover rates calculated online, demonstrates that this is a reasonable approach – as there are few differences between the gas-phase chemistry of these two models (Fig. 6). There is a lower flux of reactive halogen compounds from the 16-section represented seasalt mode than the 1-section represented seasalt mode, because the turnover rate of the smallest seasalt particles is decreased. These smallest particles become more acidic, with higher molalities of sulphuric and nitric acids (Fig. 7). But, because they do not remove these acids from the gas-aerosol system as quickly as the fixed turnover rate models, or add extra chlorine and bromine as quickly, the gas-phase H_2SO_4 and HNO_3 mixing ratios are higher, and the halogen species mixing ratios lower. It is also observed that composition gradients across the particle size-range now dominate any diurnal-variations (Fig. 7). The rapid turnover of the largest particles mean that they never equilibrate with the gas-phase and so remain alkaline, maintaining high Br^- and low SO_4^{2-} levels.

3.3 Halogen activation cycles and their impacts

Halogen activation cycles depend on the exchange of halogen species between the gas- and condensed-phases; the uptake rates of gas-phase species onto the condensed-phase are controlled by the individual species accommodation coefficients (Eq. 1). The following discussion explores the influence of changing the rate of halogen processing by the condensed-phase on gas-phase chemistry. This has been achieved

by running the 16-section S/V initialised model with three different accommodation coefficient scenarios: Base, Toyota and Low (Table 7).

The differences in gas-phase mixing ratios for these three scenarios are compared in Fig. 8. Reducing these accommodation coefficients reduces the cycling of halogens through the condensed-phase. Reducing the accommodation coefficients for the HO_x (where X=Cl, Br or I) compounds increases the gas-phase mixing ratios of HOBr, and decreases that of Br, BrO and HBr. The mixing ratios of Cl, ClO and HCl and OClO are also reduced, as well as that of HOCl. While the increase in HOBr is as expected, the reduction in HOCl seems counter-intuitive. Reducing the accommodation coefficients to the “Low” testcase further reductions in gas-phase chlorine compounds are observed, except for ClONO₂, which increases. BrONO₂ mixing ratios also increase, and all iodine compounds (except for OIO and IONO₂) decrease. The increases in XONO₂ mixing ratios result straightforwardly from the reduced accommodation coefficients slowing the uptake of these species – which also reduces the uptake of nitrogen by the condensed-phase via these heterogeneous reactions. This increases NO_x mixing ratios, although the NO_x daytime maxima in all cases are within measured mixing ratio ranges (<5 pmol mol⁻¹) of the remote MBL (cf. Torres and Thompson, 1993). At the same time reduces the halogen mixing ratios significantly below observed levels.

These changes lead to a reduction of the HO_x and XO (and cross reactions) ozone destruction cycles, but with small increases in the XONO₂ destruction cycles (Fig. 9). The HOBr and HOI cycles remain dominant, reaching maximum destruction rates of ≈0.2 and ≈0.1% hr⁻¹, while the chlorine cycles all drop to a few hundredths of a percent ozone destruction, in-line with the reduction of Cl mixing ratios to about 0.001 pmol mol⁻¹ (≈2.5 × 10⁴ molecule cm⁻³). This reduces the halogen contribution to ozone destruction to ≈0.3% hr⁻¹.

The changes observed in the gas-phase are mirrored in the condensed phase (Fig. 10). The seasalt particles take up less sulphuric and nitric acids, reducing their acidity and so reducing the activation and release of reactive chlorine and bromine across the whole size-range (though most noticeable for chlorine in the smallest par-

[Title Page](#)[Abstract](#)[Introduction](#)[Conclusions](#)[References](#)[Tables](#)[Figures](#)[◀](#)[▶](#)[◀](#)[▶](#)[Back](#)[Close](#)[Full Screen / Esc](#)[Printer-friendly Version](#)[Interactive Discussion](#)

ticles). Conversely the daytime maxima of iodine in the smallest particles increases, also due to the reduce acidity of the aerosol.

4 Conclusions

In the model sensitivity studies above, it has been demonstrated that:

- it is important to realistically represent the microphysical properties on which the modelled physical processes depend;
- where the condensed-phase acts as a chemical source, replicating the size-resolution of chemistry is less important;
- where the condensed-phase acts as an acid sink it is important to accurately represent the size-resolution of chemistry.

Thus, when considering only gas-aerosol mass-transfer processes, it is only necessary to use one size-section per aerosol mode to investigate ozone-destruction processes, provided the box-model is initialised with the correct aerosol volume and surface area. Toyota et al. (2001) observed differences between their “bulk model” and “type 1 size-segregated model” because the aerosol surface areas were not preserved in their study not because of any size-dependent chemical differences. Some physical processes, such as size-dependent turnover rates, do increase the chemical differences across the particle size-range which influence gas-phase chemistry, as demonstrated above and by the differences between the “type 1 size-segregated model” and “type 2 size-segregated model” in Toyota et al. (2001). These are, however, much less than those differences resulting from not preserving the important physical aerosol properties.

In contrast, to reproduce the temporal variations gas-phase mixing ratios of acid species such as HNO_3 and H_2SO_4 , size-resolved condensed-phase chemistry is required.

Title Page

Abstract

Introduction

Conclusions

References

Tables

Figures

◀

▶

◀

▶

Back

Close

Full Screen / Esc

Printer-friendly Version

Interactive Discussion



**Multi-phase MBL
chemistry**

D. Lowe et al.

Title Page

Abstract

Introduction

Conclusions

References

Tables

Figures

◀

▶

◀

▶

Back

Close

Full Screen / Esc

Printer-friendly Version

Interactive Discussion



Where multiple physical processes are being modelled, and so more than two aerosol microphysical properties are important, then a reduction in complexity cannot be made, and a higher aerosol size-resolution is needed. Any increase of resolution is useful, but eight or more size-sections is ideal.

To investigate halogen driven ozone-loss within a box model it is possible to use lumped chemistry bins on top of a size-resolved microphysical chemistry (e.g. von Glasow et al., 2002; Pszenny et al., 2004) without sacrificing much accuracy. However this may not hold true in non zero-dimensional models, where turbulence and gravitational mixing may exaggerate the compositional gradients across the particle size-range which can be observed even when incorporating a simple size-dependent aerosol turnover function. Further investigation in this area is needed.

Acknowledgements. This work was carried out within the EU-funded Marine Aerosol Production (MAP, GOCE 018332) and UK NERC-funded Reactive Halogens in the Marine Boundary Layer (RHAMBLE, NE/D006570/1) projects.

References

- Bott, A., Trautmann, T., and Zdunkowski, W.: A numerical model of the cloud-topped planetary boundary-layer: Radiation, turbulence and spectral microphysics in marine stratus, *Q. J. Roy. Meteorol. Soc.*, 122, 635–667, 1996. 5291
- Carver, G. D., Brown, P. D., and Wild, O.: The ASAD atmospheric chemistry integration package and chemical reaction database, *Comput. Phys. Commun.*, 105, 197–215, 1997. 5291
- Damian, V., Sandu, A., Damian, M., Potra, F., and Carmichael, G. R.: The Kinetic PreProcessor KPP – A Software Environment for Solving Chemical Kinetics, *Comput. Chem. Eng.*, 26, 1567–1579, 2002. 5292
- Graedel, T. E. and Keene, W. C.: Tropospheric budget of reactive chlorine, *Global Biogeochem. Cy.*, 9, 47–77, 1995. 5294
- Jacobson, M. Z.: Development and Application of a new Air Pollution Modeling System – II. Aerosol Module Structure and Design, *Atmos. Environ.*, 31, 131–144, 1997. 5292
- Keene, W. C., Khalil, M. A. K., Erickson, D. J., McCulloch, A., Graedel, T. E., Lobert, J. M., Aucott, M. L., Gong, S. L., Harper, D. B., Kleiman, G., Midgley, P., Moore, R. M., Seuzaret,

**Multi-phase MBL
chemistry**

D. Lowe et al.

Title Page

Abstract

Introduction

Conclusions

References

Tables

Figures

◀

▶

◀

▶

Back

Close

Full Screen / Esc

Printer-friendly Version

Interactive Discussion



- C., Turges, W. T., Benkovitz, C. M., Koropalov, V., Barrie, L. A., and Li, Y. F.: Composite global emissions of reactive chlorine from anthropogenic and natural sources: Reactive Chlorine Emissions Inventory, *J. Geophys. Res.*, 104, 8429–8440, 1999. 5290
- 5 Keene, W. C., Pszenny, A. A. P., Maben, J. R., and Sander, R.: Variation of marine aerosol acidity with particle size, *Geophys. Res. Lett.*, 29, 1101, doi:10.1029/2001GL013881, 2002. 5290
- Keene, W. C., Pszenny, A. A. P., Maben, J. R., Stevenson, E., and Wall, A.: Closure evaluation of size-resolved aerosol pH in the New England coastal atmosphere during summer, *J. Geophys. Res.*, 109, D23307, doi:10.1029/2004JD004801, 2004. 5290
- 10 Kerkweg, A., Sander, R., Tost, H., Jöckel, P., and Lelieveld, J.: Technical Note: Simulation of detailed aerosol chemistry on the global scale using MECCA-AERO, *Atmos. Chem. Phys.*, 7, 2973–2985, 2007, <http://www.atmos-chem-phys.net/7/2973/2007/>. 5293
- Pechtl, S., Lovejoy, E. R., Burkholder, J. B., and von Glasow, R.: Modeling the possible role of iodine oxides in atmospheric new particle formation, *Atmos. Chem. Phys.*, 6, 505–523, 2006, <http://www.atmos-chem-phys.net/6/505/2006/>. 5292
- 15 Porter, J. N. and Clarke, A. D.: Aerosol size distribution models based on in situ measurements, *J. Geophys. Res.*, 102, 6035–6045, 1997. 5294, 5311
- Pszenny, A. A. P., Moldanová, J., Keene, W. C., Sander, R., Maben, J. R., Martinez, M., Crutzen, P. J., Perner, D., and Prinn, R. G.: Halogen cycling and aerosol pH in the Hawaiian marine boundary layer, *Atmos. Chem. Phys.*, 4, 147–168, 2004, <http://www.atmos-chem-phys.net/4/147/2004/>. 5291, 5301
- 20 Read, K. A., Mahajan, A. S., Carpenter, L. J., Evans, M. J., Faria, B. V. E., Heard, D. E., Hopkins, J. R., Lee, J. D., Moller, S. J., Lewis, A. C., Mendes, L., McQuaid, J. B., Oetjen, H., Saiz-Lopez, A., Pilling, M. J., and Plane, J. M. C.: Extensive halogen-mediated ozone destruction over the tropical Atlantic Ocean, *Nature*, 453, 1232–1235, doi:10.1038/nature07035, 2008. 5290
- 25 Sander, R. and Crutzen, P. J.: Model study indicating halogen activation and ozone destruction in polluted air masses transported to the sea, *J. Geophys. Res.*, 101, 9121–9138, 1996. 5291, 5293
- 30 Sander, R., Keene, W. C., Pszenny, A. A. P., Arimoto, R., Ayers, G. P., Baboukas, E., Caine, J. M., Crutzen, P. J., Duce, R. A., Hönninger, G., Huebert, B. J., Maenhaut, W., Mihalopoulos, N., Turekian, V. C., and Van Dingenen, R.: Inorganic bromine in the marine boundary layer:

a critical review, *Atmos. Chem. Phys.*, 3, 1301–1336, 2003,
<http://www.atmos-chem-phys.net/3/1301/2003/>. 5290

Schwartz, S. E.: Mass-transport considerations pertinent to aqueous phase reactions of gases in liquid-water clouds, in: *Chemistry of Multiphase Atmospheric Systems*, edited by: Jaeschke, W., Springer-Verlag, New York, USA, 415–471, 1986. 5293

Slinn, S. A. and Slinn, W. G. N.: Predictions for particle deposition on natural waters, *Atmos. Environ.*, 14, 1013–1016, 1980. 5293

Sportisse, B.: An Analysis of Operator Splitting Techniques in the Stiff Case, *J. Comput. Phys.*, 161, 140–168, 2000. 5292

Topping, D., McFiggans, G., and Lowe, D.: A hybrid mixing rule/explicit thermodynamic approach for calculating gas/liquid equilibria in atmospheric aerosol particles – 1 Inorganic compounds, *J. Geophys. Res.*, 114, D04304, doi:10.1029/2008JD010099, 2009. 5292

Torres, A. L. and Thompson, A. M.: Nitric Oxide in the Equatorial Pacific Boundary Layer: SAGA 3 Measurements, *J. Geophys. Res.*, 98, 16949–16954, 1993. 5299

Toyota, K., Takahashi, M., and Akimoto, H.: Modeling multi-phase halogen chemistry in the marine boundary layer with size-segregated aerosol module: Implications for quasi-size-dependent approach, *Geophys. Res. Lett.*, 28, 2899–2902, 2001. 5291, 5293, 5294, 5300

von Glasow, R., Sander, R., Bott, A., and Crutzen, P. J.: Modeling halogen chemistry in the marine boundary layer 1. Cloud-free MBL, *J. Geophys. Res.*, 107, 4341, doi:10.1029/2001JD000942, 2002. 5291, 5294, 5301

**Multi-phase MBL
chemistry**

D. Lowe et al.

Title Page

Abstract

Introduction

Conclusions

References

Tables

Figures

◀

▶

◀

▶

Back

Close

Full Screen / Esc

Printer-friendly Version

Interactive Discussion



**Multi-phase MBL
chemistry**

D. Lowe et al.

Title Page

Abstract

Introduction

Conclusions

References

Tables

Figures

I◀

▶I

◀

▶

Back

Close

Full Screen / Esc

Printer-friendly Version

Interactive Discussion

**Table 1.** Initial gas-phase chemical mixing ratios (given in pmol mol⁻¹).

Species	mixing ratio
NO ₂	20
HCHO	300
PAN	10
CO	70 000
HNO ₃	5
SO ₂	90
CH ₃ SCH ₃	60
H ₂ O ₂	600
C ₂ H ₆	500
HCl	100
CH ₃ I	2
C ₃ H ₇ I	1
NO	10
NH ₃	50
O ₃	20 000

**Multi-phase MBL
chemistry**

D. Lowe et al.

Table 2. Gas-phase emission fluxes, $J_{e,g}$, in $\text{cm}^{-2} \text{s}^{-1}$.

Species	$J_{e,g}$
O_3	1.326×10^{12}
NO	1.5×10^9
CH_3SCH_3	2×10^9
CH_3I	6×10^6
$\text{C}_3\text{H}_7\text{I}$	1×10^7
CH_2ClI	2×10^7
CH_2I_2	3×10^7
CH_2BrI	2×10^7
I_2	40×10^7

[Title Page](#)[Abstract](#)[Introduction](#)[Conclusions](#)[References](#)[Tables](#)[Figures](#)[I◀](#)[▶I](#)[◀](#)[▶](#)[Back](#)[Close](#)[Full Screen / Esc](#)[Printer-friendly Version](#)[Interactive Discussion](#)

Table 3. Gas-phase deposition velocities, $v_{d,g}$, in cm s^{-1} .

Species	$v_{d,g}$
O ₃	1.45
H ₂ O ₂	0.5
NO ₃	1
N ₂ O ₅	1
HNO ₃	0.7
HNO ₄	0.5
HCHO	0.5
ROOH	0.5
HCl	2
HOCl	0.2
HBr	2
HOBr	0.2
CH ₃ SOCH ₃	0.5
DMSO ₂	0.5
SO ₂	0.87
H ₂ SO ₄	1
HI	1
HOI	1
INO ₃	1
INO ₂	1
HCOOH	1

**Multi-phase MBL
chemistry**

D. Lowe et al.

Title Page

Abstract

Introduction

Conclusions

References

Tables

Figures

◀

▶

◀

▶

Back

Close

Full Screen / Esc

Printer-friendly Version

Interactive Discussion



**Multi-phase MBL
chemistry**

D. Lowe et al.

Table 4. Parameters for the non-seasalt aerosol distribution used in study. N_{tot} is in cm^{-3} and R_N in μm . The log-normal particle size distribution is calculated according to

$$\frac{dN(r)}{dr} = \frac{N_{\text{tot}}}{\lg \sigma \sqrt{2\pi}} \times \exp\left(-\frac{(\lg r - \lg R_N)^2}{2(\lg \sigma)^2}\right).$$

Mode	N_{tot}	R_N	σ
non-seasalt	237	0.088	1.29

[Title Page](#)[Abstract](#)[Introduction](#)[Conclusions](#)[References](#)[Tables](#)[Figures](#)[I◀](#)[▶I](#)[◀](#)[▶](#)[Back](#)[Close](#)[Full Screen / Esc](#)[Printer-friendly Version](#)[Interactive Discussion](#)

Multi-phase MBL
chemistry

D. Lowe et al.

Table 5. Comparison of the initial total moments (number, surface area and volume) of the seasalt mode for the three different initialisation methods (N/S, N/V and S/V). The surface areas and volumes are for the “dry” aerosol (i.e. without water). See text for details of initialising the seasalt mode.

	Number of Sections	Number ($\text{cm}_{\text{air}}^{-3}$)	Dry Surface Area ($\mu\text{m}^2 \text{cm}_{\text{air}}^{-3}$)	Dry Volume ($\mu\text{m}^3 \text{cm}_{\text{air}}^{-3}$)
N/S	1	8.797	12.68	1.432
	4	8.797	12.68	5.600
	16	8.797	12.68	6.736
	1	8.797	36.00	6.847
N/V	4	8.797	14.76	6.847
	16	8.797	12.82	6.847
	1	0.385	12.68	6.847
S/V	4	5.735	12.68	6.847
	16	8.514	12.68	6.847

Title Page

Abstract

Introduction

Conclusions

References

Tables

Figures

I◀

▶I

◀

▶

Back

Close

Full Screen / Esc

Printer-friendly Version

Interactive Discussion



**Multi-phase MBL
chemistry**

D. Lowe et al.

Table 6. Volumetrically-averaged seasalt aerosol turnover rates.

Size-resolution (no. of sections)	Aerosol lifetime (days)	Turnover rate (s ⁻¹)
1	2.66	0.44×10^{-5}
2	1.31	0.88×10^{-5}
4	0.77	1.50×10^{-5}
8	0.61	1.90×10^{-5}
16	0.57	2.03×10^{-5}

[Title Page](#)[Abstract](#)[Introduction](#)[Conclusions](#)[References](#)[Tables](#)[Figures](#)[I◀](#)[▶I](#)[◀](#)[▶](#)[Back](#)[Close](#)[Full Screen / Esc](#)[Printer-friendly Version](#)[Interactive Discussion](#)

**Multi-phase MBL
chemistry**

D. Lowe et al.

Table 7. Accommodation coefficients of key halogen species used in the three different scenarios.

Species	Accommodation Coefficients		
	Pechtl	Toyota	Low
HOCl	0.5	0.01	0.01
ClONO ₂	0.1	0.1	0.01
HOBr	0.5	0.01	0.01
BrONO ₂	0.8	0.8	0.01
HOI	0.5	0.01	0.01
IONO ₂	0.1	0.1	0.01
OIO	1.0	1.0	0.01

[Title Page](#)[Abstract](#)[Introduction](#)[Conclusions](#)[References](#)[Tables](#)[Figures](#)[I◀](#)[▶I](#)[◀](#)[▶](#)[Back](#)[Close](#)[Full Screen / Esc](#)[Printer-friendly Version](#)[Interactive Discussion](#)

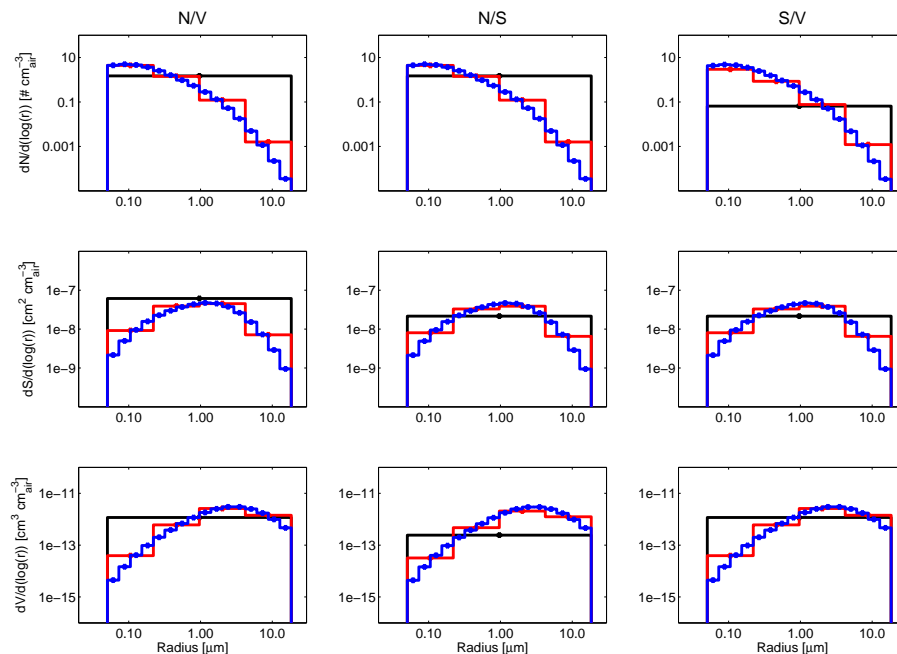


Fig. 1. Comparison of the moments (number, surface area and volume) of the sea salt mode, using the Porter and Clarke (1997) based distribution, when using the three different initialisation methods (NV, NS and SV). Blue, red and black lines represent the 16-, 4-, and 1-section distributions, respectively.

[Title Page](#)
[Abstract](#)
[Introduction](#)
[Conclusions](#)
[References](#)
[Tables](#)
[Figures](#)
[◀](#)
[▶](#)
[◀](#)
[▶](#)
[Back](#)
[Close](#)
[Full Screen / Esc](#)
[Printer-friendly Version](#)
[Interactive Discussion](#)

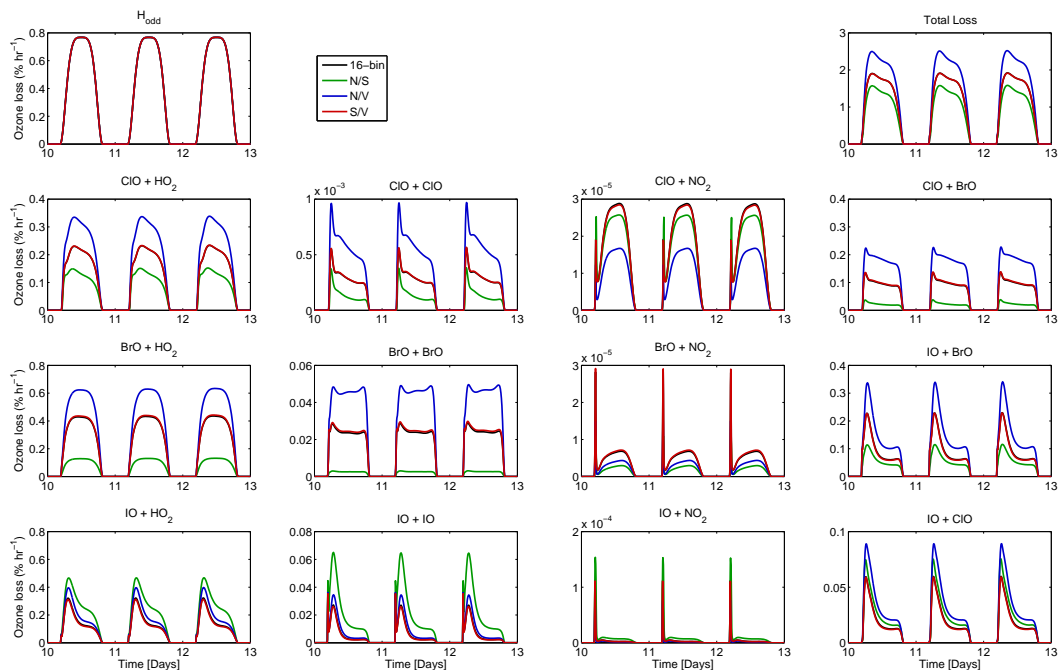



Fig. 2. Comparison of ozone destruction rates (in percentage of total ozone per hour) for the 16-section S/V initialised seasalt mode, and the 1-section N/S, N/V, and S/V initialised seasalt modes. These are represented by the black, green, blue and red lines, respectively. The seasalt aerosol turnover rate is fixed at 0.57 days (see text).

[Title Page](#)
[Abstract](#)
[Introduction](#)
[Conclusions](#)
[References](#)
[Tables](#)
[Figures](#)
[◀](#)
[▶](#)
[◀](#)
[▶](#)
[Back](#)
[Close](#)
[Full Screen / Esc](#)
[Printer-friendly Version](#)
[Interactive Discussion](#)


Multi-phase MBL
chemistry

D. Lowe et al.

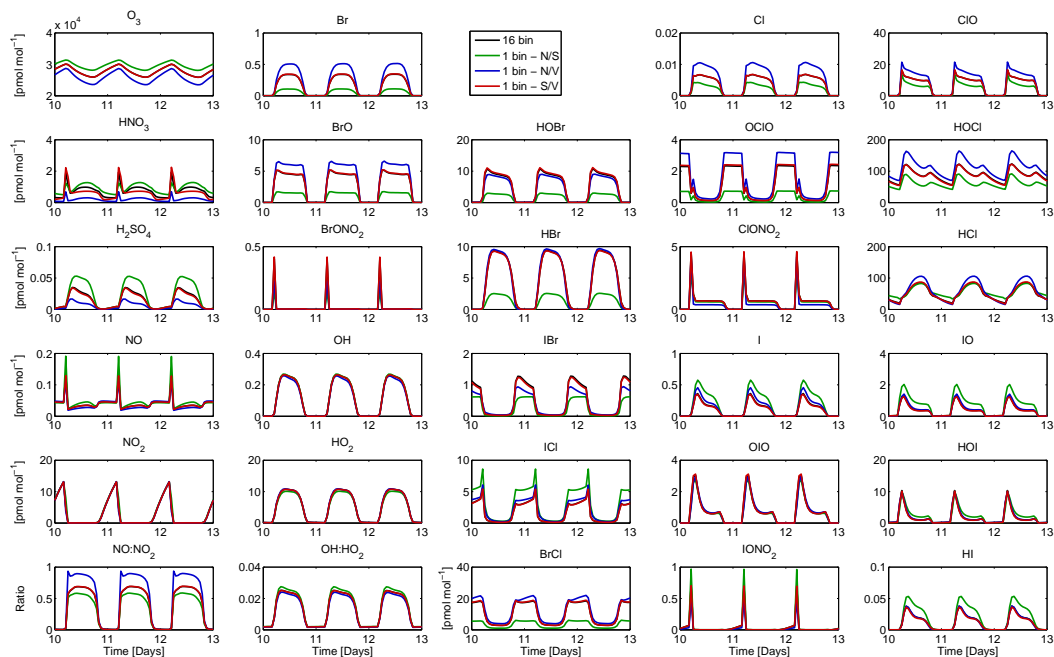


Fig. 3. Comparison of gas-phase mixing ratios for ozone, the major halogen species, and the major HO_x and NO_x species for the 16-section S/V initialised seasalt mode, and the 1-bin N/S, N/V, and S/V initialised seasalt modes. These are represented by the black, green, blue and red lines, respectively. The seasalt aerosol turnover rate is fixed at 0.57 days (see text).

Title Page

Abstract

Introduction

Conclusions

References

Tables

Figures

◀

▶

◀

▶

Back

Close

Full Screen / Esc

Printer-friendly Version

Interactive Discussion



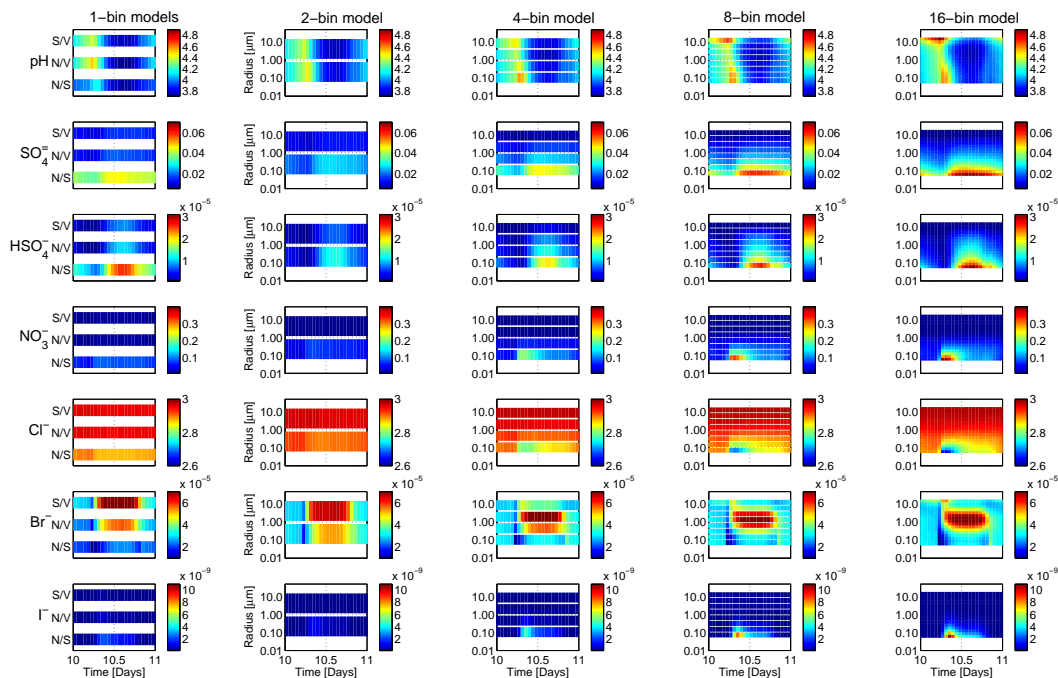


Fig. 4. Comparison of pH and nitrate, sulphate and halogen molalities of the 1-section S/V, N/V and N/S initialised, and 2-, 4-, 8-, and 16-section S/V initialised seasalt modes. The seasalt aerosol turnover rate is fixed at 0.57 days (see text).

Multi-phase MBL chemistry

D. Lowe et al.

Title Page

Abstract

Introduction

Conclusions

References

Tables

Figures

◀

▶

◀

▶

Back

Close

Full Screen / Esc

Printer-friendly Version

Interactive Discussion



Multi-phase MBL
chemistry

D. Lowe et al.

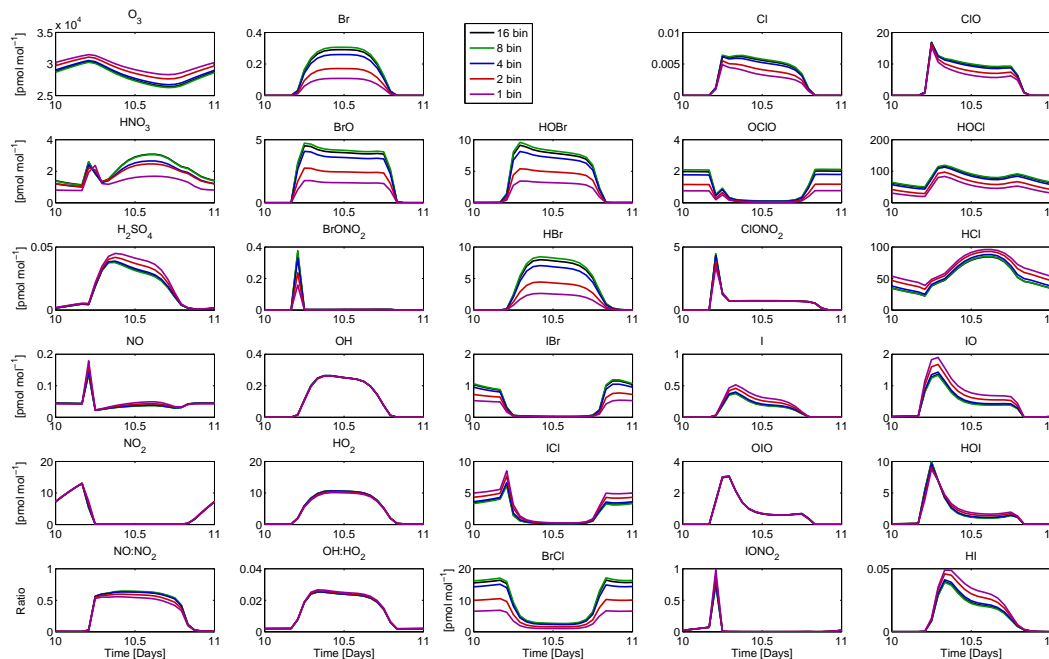


Fig. 5. Comparison of gas-phase mixing ratios for ozone, the major halogen species, and the major HO_x and NO_x species for the 16-, 8-, 4-, 2-, and 1-section S/V initialised seasalt modes. These are represented by the black, green, blue, red, and purple lines, respectively. The seasalt aerosol turnover rate is calculated on-line for each different size-resolution.

Title Page

Abstract

Introduction

Conclusions

References

Tables

Figures

◀

▶

◀

▶

Back

Close

Full Screen / Esc

Printer-friendly Version

Interactive Discussion



Multi-phase MBL
chemistry

D. Lowe et al.

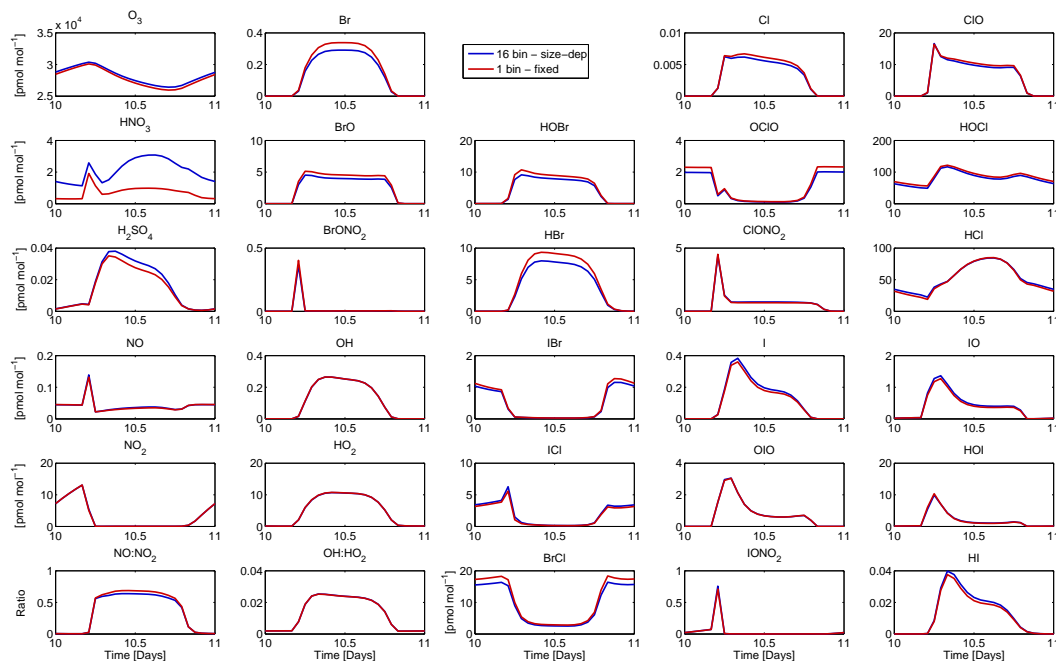


Fig. 6. Comparison of gas-phase mixing ratios for ozone, the major halogen species, and the major HO_x and NO_x species for the 16-, and 1-section S/V initialised seasalt modes. These are represented by the blue and red lines, respectively. The seasalt aerosol turnover rate is calculated on-line for the 16-section seasalt mode, for the 1-section seasalt mode the turnover rate is fixed at 0.57 days.

Title Page

Abstract

Introduction

Conclusions

References

Tables

Figures

◀

▶

◀

▶

Back

Close

Full Screen / Esc

Printer-friendly Version

Interactive Discussion



Multi-phase MBL
chemistry

D. Lowe et al.

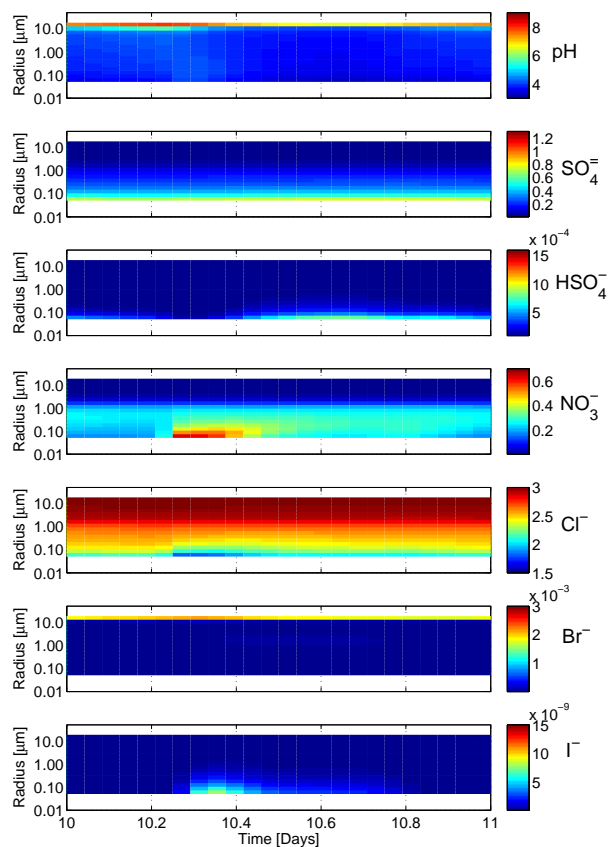


Fig. 7. pH and nitrate, sulphate and halogen molalities for the 16-section S/V initialised seasalt mode. The seasalt aerosol turnover rate is calculated on-line.

[Title Page](#)[Abstract](#)[Introduction](#)[Conclusions](#)[References](#)[Tables](#)[Figures](#)[◀](#)[▶](#)[◀](#)[▶](#)[Back](#)[Close](#)[Full Screen / Esc](#)[Printer-friendly Version](#)[Interactive Discussion](#)

Multi-phase MBL
chemistry

D. Lowe et al.

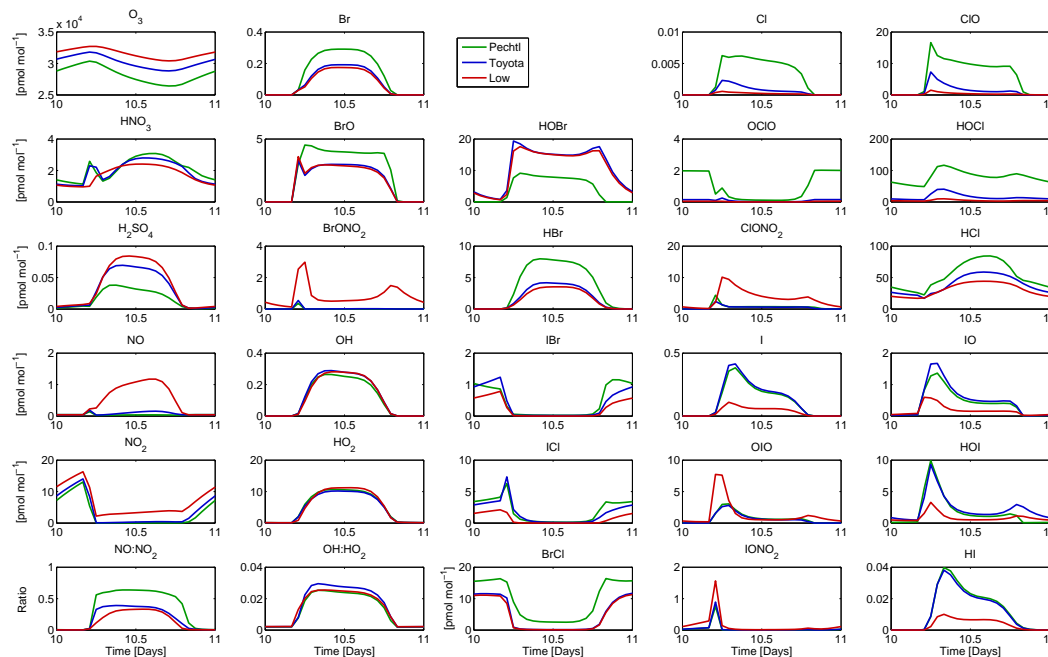


Fig. 8. Comparison of gas-phase mixing ratios for ozone, the major halogen species, and the major HO_x and NO_x species for the 16-section S/V initialised seasalt mode using the Pechtl, Toyota, and Low accommodation coefficient settings. These are represented by the green, blue and red lines, respectively. The seasalt aerosol turnover rate is calculated on-line.

Title Page

Abstract

Introduction

Conclusions

References

Tables

Figures

◀

▶

◀

▶

Back

Close

Full Screen / Esc

Printer-friendly Version

Interactive Discussion



Multi-phase MBL
chemistry

D. Lowe et al.

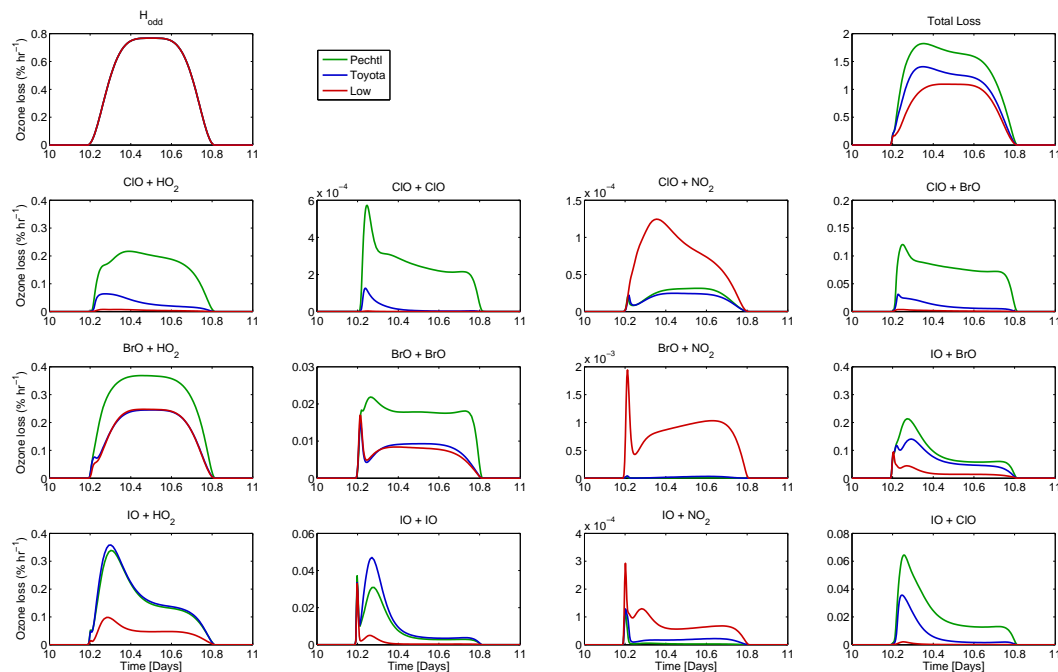


Fig. 9. Comparison of ozone destruction rates (in percentage of total ozone per hour) for the 16-section S/V initialised seasalt mode using the Pechtl, Toyota, and Low accommodation coefficient settings. These are represented by the green, blue and red lines, respectively. The seasalt aerosol turnover rate is calculated on-line.

Title Page

Abstract

Introduction

Conclusions

References

Tables

Figures

◀

▶

◀

▶

Back

Close

Full Screen / Esc

Printer-friendly Version

Interactive Discussion



Multi-phase MBL
chemistry

D. Lowe et al.

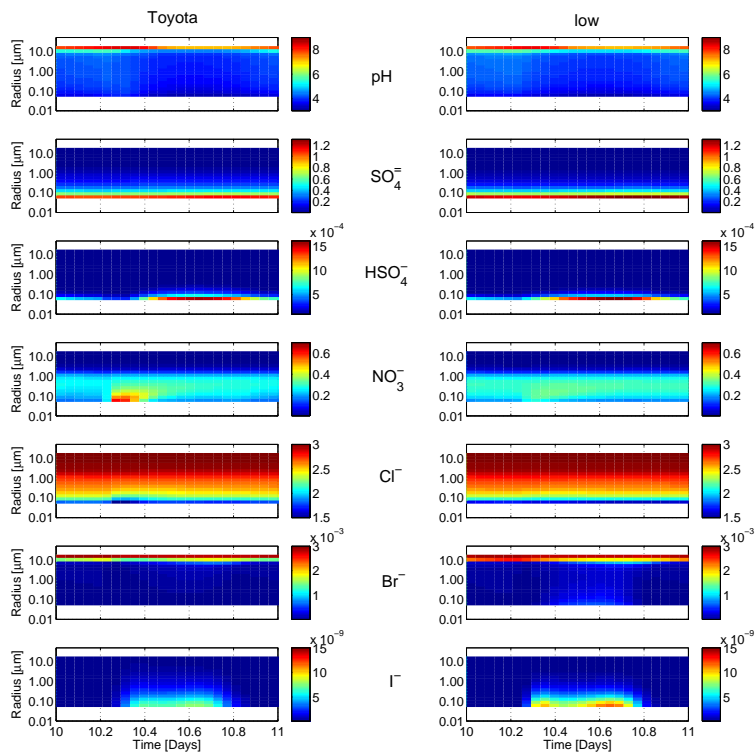


Fig. 10. Comparison of pH and nitrate, sulphate and halogen molalities of the 16-section S/V initialised seasalt mode using the Toyota, and Low accommodation coefficient settings. The pH and molality data for the Pechtl setting are shown in Fig. 7 (using the same colour scales). The seasalt aerosol turnover rate is calculated on-line.

Title Page

Abstract

Introduction

Conclusions

References

Tables

Figures

◀

▶

◀

▶

Back

Close

Full Screen / Esc

Printer-friendly Version

Interactive Discussion

